BRAIN
ORIGINAL ARTICLE

Glycogen synthase downregulation rescues the amylopectinosis of murine RBCK1 deficiency

Silvia Nitschke,[1,2,†] Mitchell A. Sullivan,[1,3,†] Sharmistha Mitra,[2] Charlotte R. Marchioni,[2] Jennifer P. Y. Lee,[1] Brandon H. Smith,[2] Saija Ahonen,[1] Jun Wu,[2] Erin E. Chown,[1] Peixiang Wang,[1] Sara Petković,[1] Xiaochu Zhao,[1] Laura F. DiGiovanni,[1] Ami M. Perri,[1] Lori Israelian,[1] Tamar R. Grossman,[4] Holly Kordasiewicz,[4] Francisco Vilaplana,[5] Kazuhiro Iwai,[6] Felix Nitschke[2,7] and Berge A. Minassian[1,2]

[†]These authors contributed equally to this work.

Longer glucan chains tend to precipitate. Glycogen, by far the largest mammalian glucan and the largest molecule in the cytosol with up to 55 000 glucoses, does not, due to a highly regularly branched spherical structure that allows it to be perfused with cytosol. Aberrant construction of glycogen leads it to precipitate, accumulate into polyglucosan bodies that resemble plant starch amylopectin and cause disease. This pathology, amylopectinosis, is caused by mutations in a series of single genes whose functions are under active study toward understanding the mechanisms of proper glycogen construction. Concurrently, we are characterizing the physicochemical particularities of glycogen and polyglucosans associated with each gene. These genes include *GBE1*, *EPM2A* and *EPM2B*, which respectively encode the glycogen branching enzyme, the glycogen phosphatase laforin and the laforin-interacting E3 ubiquitin ligase malin, for which an unequivocal function is not yet known. Mutations in *GBE1* cause a motor neuron disease (adult polyglucosan body disease), and mutations in *EPM2A* or *EPM2B* a fatal progressive myoclonus epilepsy (Lafora disease). RBCK1 deficiency causes an amylopectinosis with fatal skeletal and cardiac myopathy (polyglucosan body myopathy 1, OMIM# 615895). RBCK1 is a component of the linear ubiquitin chain assembly complex, with unique functions including generating linear ubiquitin chains and ubiquitinating hydroxyl (versus canonical amine) residues, including of glycogen.

In a mouse model we now show (i) that the amylopectinosis of RBCK1 deficiency, like in adult polyglucosan body disease and Lafora disease, affects the brain; (ii) that RBCK1 deficiency glycogen, like in adult polyglucosan body disease and Lafora disease, has overlong branches; (iii) that unlike adult polyglucosan body disease but like Lafora disease, RBCK1 deficiency glycogen is hyperphosphorylated; and finally (iv) that unlike laforin-deficient Lafora disease but like malin-deficient Lafora disease, RBCK1 deficiency's glycogen hyperphosphorylation is limited to precipitated polyglucosans.

In summary, the fundamental glycogen pathology of RBCK1 deficiency recapitulates that of malin-deficient Lafora disease. Additionally, we uncover sex and genetic background effects in RBCK1 deficiency on organ- and brain-region specific amylopectinoses, and in the brain on consequent neuroinflammation and behavioural deficits. Finally, we exploit the portion of the basic glycogen pathology that is common to adult polyglucosan body disease, both forms of Lafora disease and RBCK1 deficiency, namely overlong branches, to show that a unified approach based on downregulating glycogen synthase, the enzyme that elongates glycogen branches, can rescue all four diseases.

1 Program in Genetics and Genome Biology, The Hospital for Sick Children Research Institute, Toronto, ON M5G 0A4, Canada

Received October 29, 2021. Revised December 17, 2021. Accepted January 9, 2022. Advance access publication January 27, 2022

2 Division of Neurology, Department of Pediatrics, University of Texas Southwestern Medical Center, Dallas, TX 75390, USA
3 Glycation and Diabetes Complications, Mater Research Institute–The University of Queensland, Translational Research Institute, Brisbane, QLD, 4102, Australia
4 Department of Antisense Drug Discovery, Ionis Pharmaceuticals, Carlsbad, California, USA
5 Division of Glycoscience, Department of Chemistry, KTH Royal Institute of Technology, AlbaNova University Centre, Stockholm 10691, Sweden
6 Department of Molecular and Cellular Physiology, Kyoto University School of Medicine, Kyoto 606-8501, Japan
7 Department of Biochemistry, University of Texas Southwestern Medical Center, Dallas, TX 75390, USA

Correspondence to: Dr Berge A. Minassian
University of Texas Southwestern Medical Center
Dallas, TX 75390-9063, USA
E-mail: berge.minassian@utsouthwestern.edu

Correspondence may also be addressed to: Dr Felix Nitschke
E-mail: felix.nitschke@utsouthwestern.edu

Keywords: PGBM1 (polyglucosan body myopathy 1); antisense oligonucleotide (ASO) therapy; neuroinflammation; glycogen synthase; RBCK1/HOIL1

Abbreviations: APBD = adult polyglucosan body disease; ASO = antisense oligonucleotide; C6 = carbon six; CLD = chain length distribution; LD = Lafora disease; LUBAC = linear ubiquitin chain assembly complex; MSD = molecule size distribution; PASD = periodic acid–Schiff diastase; PB = polyglucosan body; RD = RBCK1 deficiency; WT = wild-type

Introduction

Circulating glucose is the most direct source of energy for the brain and other organs. Lipids are the most indirect, are stored externally in adipose tissue and are mobilized slowly. Glycogen occupies an intermediate position; it is stored, soluble, in the cytosol for rapid glucose provision by glycogen-digesting enzymes glycogen phosphorylase and glycogen debranching enzyme.

Glucose chains exceeding 10 units form double helices that extrude water and precipitate,[1] yet glycogen with up to ≈55 000 glucose units is soluble. Solubility has long been thought to be achieved solely through the balanced activities of the glycogen-synthesizing enzymes glycogen synthase (GYS) and glycogen branching enzyme (GBE1), as follows. While GYS extends a glucan chain, GBE1 cleaves part of the extended chain and reattaches it *en bloc* upstream, thus converting the linear chain to a fork. GYS now elongates each prong, which GBE1 cleaves and branches, and so forth. The final product is highly branched with short branches pointing away from each other, allowing the macromolecule to be perfused with cytosol and remain in solution.[2,3] In patients with mutations that lead to GBE1 deficiency, GYS outpaces GBE1, and glycogen with overly long branches forms (termed polyglucosan), which resembles the main component of starch, amylopectin. Polyglucosans precipitate, cannot be digested, accumulate into masses called polyglucosan bodies (PBs; amylopectinosis) and lead to disease. Because glycogen is ubiquitous, PBs form in most organs, but not all are affected clinically. The range of organs exhibiting clinical disease depends on mutation type, depth of GBE1 deficiency and corresponding extent of amylopectinosis. The most common *GBE1* mutations lead to an adult-onset disease clinically limited to the nervous system and resembling amyotrophic lateral sclerosis, namely adult polyglucosan body disease (APBD).[4–7]

Lafora disease (LD) and RBCK1 deficiency (RD; polyglucosan body myopathy 1, PGBM1) are diseases with amylopectinosis where the causative deficient proteins are not the classical enzymes of glycogen synthesis. This suggests the existence of unknown mechanisms beyond balanced GYS/GBE1 activities in glycogen architecture. LD is a fatal progressive myoclonus epilepsy caused by mutations in the *EPM2A* (laforin) or *EPM2B* (malin) genes.[8,9] Laforin is a phosphatase that dephosphorylates glycogen.[10,11] Malin is a laforin-interacting partner and an E3 ubiquitin ligase[12] whose physiological substrate remains unknown.[3] RD is a disabling skeletal myopathy and usually, unless transplanted, a fatal cardiomyopathy.[13–16] A subset of RD patients additionally has immune dysregulation manifesting as a paradoxical hyperinflammatory immunodeficiency.[15–17] RBCK1 (also called HOIL1) is an E3 ubiquitin ligase that combines with two other proteins, SHARPIN and HOIP (another E3 ubiquitin ligase), to form the linear ubiquitin chain assembly complex (LUBAC).[18–24] This complex, primarily through HOIP's ligase activity, generates unique linear methionine-linked ubiquitin chains (as opposed to standard non-linear lysine-linked chains).[25,26] RBCK1 participates by (i) ensuring the structural integrity of LUBAC[24,27]; (ii) monoubiquitinating itself and the other two LUBAC components to regulate the complex's activity[28]; (iii) placing the first ubiquitin in the linear chain to be formed by HOIP[29]; and (iv) incorporating ubiquitins into the growing linear chains.[30] RBCK1 is a highly unusual E3 ligase in one more way. It is capable of catalysing ubiquitination of hydroxyl (OH) residues (in addition to canonical amine groups).[30–32] In most recent results tantalizing to the present study, this property of ubiquitinating OH groups appears to extend also to glycogen, at least *in vitro*.[33] While co-localization of ubiquitin with PBs has been demonstrated in human, murine, and canine LD,[34–37] a recent study in RD patients also confirmed the presence of ubiquitin in RD-related PBs.[38]

Toward elucidating the unknown mechanisms in the shaping of glycogen, and of amylopectinosis, we and others previously uncovered the characteristics of soluble and insoluble glycogen specific to APBD and LD. These are detailed below. Briefly here, there are important physicochemical differences in glycogen and polyglucosans between APBD and LD, and also between the two forms of LD.

Despite these differences, all three share a common path to glycogen precipitation, namely the formation of overlong glycogen branches.[39] This convergent critical pathology led to a therapeutic approach, downregulating GYS, which rescued the mouse models of these diseases and is underway toward clinical trial.[40–49] In the present work, we characterize the glycogen and polyglucosan of RD in the same fashion. We find that RD glycogen and polyglucosans recapitulate those of the malin deficiency form of LD. As such, the same final path to glycogen precipitation applies also to RD. We proceed to show that the same therapeutic strategy, downregulating GYS1 by genetic or pharmaceutical means, also rescues murine RD.

Materials and methods

Mice

The LUBAC complex assembles through the interactions of the ubiquitin-like (UBL) domains of RBCK1 and SHARPIN with the ubiquitin-associated domains of HOIP.[23,24] Loss of any of its three members leads to disintegration not only of the complex but also the other two proteins.[24] *Rbck1* null mice are embryonic-lethal.[24,50] Prior to this being known, Tokunaga *et al.* generated a mouse line in which exon 7 and part of exon 8 of the 12 exons of *Rbck1* were replaced with a neomycin resistance cassette. This disrupted RBCK1's E3 ubiquitin ligase domain and led to complete loss of full-length RBCK1. Yet these mice survived.[51] It was later shown that an N-terminal portion of the protein containing the UBL domain was still present, possibly the product of a splice variant of the gene not affected by the mutation, or because of incomplete nonsense-mediated mRNA decay (NMD). This truncated RBCK1 was able to stabilize LUBAC, although in greatly diminished amount.[24] In summary, the Tokunaga *et al.* mice have a small amount of LUBAC that lacks RBCK1's E3 ubiquitin ligase domain. These are the mice used in the present study and referred to as $Rbck1^{-/-}$.

Gys1 encodes GYS in skeletal muscle, heart, and brain.[52] *Ppp1r3c* encodes the ubiquitously expressed PTG protein, which targets protein phosphatase 1 to dephosphorylate and activate GYS.[53,54] $Rbck1^{+/-}$ mice were either intercrossed to obtain wild-type and $Rbck1^{-/-}$ littermates or crossed with knockouts of *Gys1* [$Gys1^{tm1a(EUCOMM)Wtsi}$][46] or $Ppp1r3c$[40] to obtain $Rbck1^{-/-}$ mice with mono-allelic *Gys1* knockout or bi-allelic *Ppp1r3c* knockout. Wild-type and $Gys1^{+/-}$ or $Ppp1r3c^{-/-}$ littermates were used as controls. Mice were housed in ventilated cages at 21 ± 1°C, under a 12-h light–dark cycle with *ad libitum* access to a standard diet and water. Unless otherwise stated, mice were sacrificed by cervical dislocation and harvested brain, heart, skeletal muscle and liver tissues were divided, half fixed in neutral buffered formalin (10%) and half snap-frozen in liquid nitrogen. Spinal cords were removed and fixed in neutral buffered formalin. Unless otherwise indicated, mice were sacrificed at 14–16 months. All animal procedures were approved by the Toronto Centre for Phenogenomics Animal Care Committee.

ASO delivery

Antisense oligonucleotides (ASOs) were synthesized and screened as described.[49] Isofluorane-anaesthetized mice were intracerebroventrically injected with 300 µg of a *Gys1*-targeting ASO (5′-GCCACAGCCTGGAAGCCAAT-3′) in 10 µl phosphate-buffered saline (PBS) at 1 and 2 months of age, alternating ventricles at successive time points. Stereotactic injection coordinates were 0.3 mm anterior/posterior (anterior to bregma), 1.0 mm to right or left medial/lateral and −3.0 mm dorsal/ventral. Analgesic (Metacam 2 mg/kg) was administered before and for 2 days post injections. Littermate controls were injected with a no-target ASO, 5′-CCTATAGGACTATCCAGGAA-3′ (Ctrl-ASO), or PBS. Mice were sacrificed at 3 months by cervical dislocation and brains were harvested. One-month-old non-injected mice served as additional controls (baseline).

Gys1 expression analysis

Brain tissue was homogenized using a 1 cm^3 syringe and 21 g needle and RNA extracted using the Qiagen RNeasy Lipid Tissue Mini Kit (Qiagen, #74804). DNA was digested with DNase I (Thermo Scientific, #EN0521). cDNA was synthesized from 1 µg RNA using the iScript Advanced cDNA Synthesis Kit (Bio-Rad, #1725037).

For quantitative real-time polymerase chain reaction (qRT-PCR) the Stratagene Mx3005P (Agilent Technologies) real-time polymerase chain reaction (PCR) system and SYBR Green technology [PowerUp SYBR Green Master Mix (Applied Biosystems, A25741)] were used. Primer sequences were Gys1-F: 5′-CGCAAACAACTATGGGACAC-3′, Gys1-R: 5′-TCCTCCTTGTCCAGCATCTT-3′, Gapdh-F: 5′-AAGGGCTCATGACCACAGTC-3′, and Gapdh-R: 5′-GGATGCAGGGATGATGTTCT-3′. *Gapdh* served as reference gene. Delta cycle threshold (ΔCt) values were determined, calculating $Ct_{gene\ of\ interest}$–$Ct_{reference\ gene}$, followed by transformation into $2^{-\Delta Ct}$. Expression levels were further normalized to the PBS group.

Behavioural analyses

Mice were acclimatized to the behavioural testing room for 30 min prior to testing.

Balance beam

The time taken for mice to traverse a cylindrical balance beam (90 cm long, 18 mm diameter) suspended 50 cm above the floor was recorded (cut-off limit set to 60 s). Mice underwent four consecutive training trials the day prior to testing. For experiments with $Rbck1^{-/-}$ $Gys1^{+/-}$ and $Rbck1^{-/-}$ $Ppp1r3c^{-/-}$ mice, hind feet slips were additionally recorded.

Grip strength

Maximum forelimb grip strength (peak tension) was measured using the Animal Grip Strength System (San Diego Instruments). Mice underwent five consecutive trials and all scores were averaged.

Rotarod

An accelerating rotarod (4–40 rpm over 300 s) was used to assess motor coordination. Latency to fall or to complete two passive rotations was measured. Each mouse performed four trials with a 30-min inter-trial interval. The longest three of four scores were averaged.

Open field test

The open field test evaluates anxiety and exploratory behaviour. A sound-attenuating open field arena (43.2 cm^2) fitted with three 16 beam IR arrays (*x*, *y* and *z* axes) and 275 lx LED lights was used with activity monitoring software. The arena was divided into a peripheral zone (8 cm from the edge of each wall) and a brightly illuminated central zone (around 40% of the total area). Mice were

placed in the middle of the apparatus in the dark. Testing was initiated when the light turned on, and distance travelled, number of rears and percent time spent in the centre zone were recorded for 20 min. No differences were detected between genotypes, the distance travelled being shown as one example.

Vertical pole

The vertical pole test was performed as previously described.[55,56] Mice were placed on a rough-surfaced vertical pole (45 cm high, 1.1 cm in diameter). The time for each mouse to turn downward (t1) and the total time to reach the floor (t2) were recorded (t2 cut-off limit being set to 120 s). Each mouse performed three trials. The difference between t2 and t1 was averaged across the trials.

Gait analysis

The ExerGait (XL) treadmill (Columbus Instruments) was used to analyse gait. Treadmill speed was set to 19 cm/s and the camera frame rate to 100 frames/s with a maximum of 2000 frames taken. Mice were placed on the non-moving treadmill for 30 s to acclimatize. Recording commenced once the treadmill was turned on and mice reached a constant running pace. Test duration was 20 s. If the mouse's running pace oscillated, the procedure was restarted. The collected video was analysed using TreadScan software (Clever Sys Inc).

Histological analyses

Formalin-fixed paraffin-embedded brain tissues were sectioned and stained using (i) periodic acid–Schiff after diastase treatment (PASD) to visualize PBs[40]; or (ii) immunohistochemistry against glial fibrillary acidic protein (GFAP; mouse anti-GFAP, BioGenex, #AM020-5M; dilution 1:250) or IBA1 (rabbit anti-IBA1, Wako, #01919741; dilution 1:1400). Slides were scanned using the Panoramic (3DHistech) slide scanner. PB, GFAP and IBA1 signals were quantified in the hippocampus and cerebellum using HistoQuant (3DHistech) by defining respective signals based on pixel colour. Values are expressed as % area.

For co-immunostainings, isoflurane-anaesthetized mice were sacrificed by transcardial perfusion (20 ml ice-cold PBS followed by 20 ml ice-cold 4% paraformaldehyde in PBS). Dissected brains were fixed in ice-cold 4% paraformaldehyde in PBS for 3 h, rinsed in PBS and transferred to 30% sucrose in PBS. Tissues were embedded in Tissue-Tek OCT compound (Sakura Finetek USA, Inc) and sectioned (15 µm) using the Leica CM1950 cryostat. Free-floating coronal brain sections (in PBS with 0.05% sodium azide) were used. These were blocked with 5% normal donkey serum plus 0.1% Triton X-100 in PBS for 2 h and incubated for 48 h at 4°C with primary antibodies diluted in blocking solution. Antibody against GYS1 (rabbit, 1:400, ab40810, Abcam) was used with antibody against GFAP (mouse, 1:500, BD556330, BD bioscience). The sections were then washed with 0.1% Triton X-100 in PBS and incubated overnight at 4°C with secondary antibodies diluted in blocking buffer: AF 488 donkey anti-mouse (1:1000, A-21202, ThermoFisher), AF 488 donkey anti-goat (1:800, A-11055, ThermoFisher) and AF 594 donkey anti-rabbit (1:1000, A-21207, ThermoFisher). After incubation with DAPI, sections were mounted using Aqua-Poly/Mount (Polysciences, Inc). Images of the different brain regions were taken on Zeiss LSM 780 inverted confocal at 40× magnification (zoom factor 0.6) with z-stack of 0.45 µm.

Western blot analyses

Frozen brain tissue was homogenized with extraction buffer including Pierce protease and phosphatase inhibitors (Thermo Scientific) and 2 mM dithiothreitol.[39] Protein concentrations were determined using the DC Protein Assay (Bio-Rad). Equal protein amounts (20 µg) from homogenates (total), supernatants (soluble) and resuspended pellets (insoluble) were heated in sample buffer (70°C, 10 min) and loaded to 10% sodium dodecyl sulphate–polyacrylamide gel electrophoresis for separation. Proteins were transferred to nitrocellulose membranes and blocked with 5% skimmed milk. Subsequently, the membrane was probed with commercial primary antibodies GYS1 (Cell signalling #3886 from rabbit), GBE1 (Abcam, #ab180596 from rabbit), or laforin (EPM2A, Abnova #H00002632 from mouse), actin (BD Transduction Laboratories #612657 from mouse). Immunoblots were detected with horse radish peroxidase-conjugated secondary antibodies and Clarity Western ECL-substrate (Bio-Rad) and analysed with the ChemiDoc Imaging system (Bio-Rad).

Muscle glycogen separation

Glycogen separation into soluble and insoluble glycogen was performed as previously described[39] with a few exceptions: (i) 200 mg of frozen ground muscle tissue from wild-type and *Rbck1*$^{-/-}$ mice were used and homogenized in 2 ml of glycogen isolation buffer; (ii) Triton X-100 was added to homogenates (initially 0.95%), and recurrent vortexing for 15 min was conducted to optimize separation of soluble and insoluble glycogen; (iii) an additional wash cycle to completely remove contaminants derived from the soluble fraction was added yielding supernatant 6 (S6), which was devoid of free or glycogen-derived glucose; (iv) aliquots of each fraction, total (homogenate), soluble (supernatant 1), S6 as negative control and insoluble (pellet) were taken, the Triton X-100 concentration was adjusted (to be equal in each fraction) and a heat treatment step was added prior to glycogen content analysis to eliminate all enzymatic activities; and (v) only glycogen from the soluble and insoluble fractions was further purified and analyzed for chain length distribution (CLD) and molecule size distribution (MSD) analyses.

Glycogen analyses

Glycogen extraction, amyloglucosidase digestion and glucose determination were conducted as previously described.[57] For glycogen carbon 6 (C6) phosphate determination as well as CLD and MSD analyses protocols from Sullivan *et al.* were followed.[39]

Statistical analyses

Data are presented as mean ± SEM, except for CLD and MSD analyses where mean ± SD is displayed. Biological replicates are indicated by individual data-points and are given for each panel in the figure legend. Statistics were performed with GraphPad Prism 8.4.3. For Figs 1–3 a parametric unpaired two-tailed *t*-test with Welch's correction was used. Exceptions are Figs 1I, 3G, J and K showing glycogen CLD and MSD analyses. Here, significance between genotypes was tested for each individual degree of polymerization and hydrodynamic radius, respectively, by using one-way ANOVA, followed by *post hoc* tests with Holm–Bonferroni multiple comparison correction. For all four-genotype comparisons two-way ANOVA was performed, followed by *post hoc* tests with Tukey multiple comparison correction. For heart glycogen analyses, two-

way ANOVA and *post hoc* tests were followed by two-stage linear step-up procedure of Benjamini, Krieger and Yekutieli. For behavioural analyses with three genotypes and the ASO data, one-way ANOVA was performed, followed by *post hoc* tests with Tukey multiple comparison correction. Statistical analyses with $P > 0.05$ were considered non-significant. Asterisks denote statistical significance as follows: *$P < 0.05$; **$P < 0.01$; ***$P < 0.001$; ****$P < 0.0001$.

Data availability

The study's raw data are available upon request.

Results

Rbck1$^{-/-}$ mice exhibit amylopectinosis in the CNS

PBs were first seen in 1911 in the brain in LD.[58] Between 1955 and 1965, they were shown to also be present in the heart, skeletal muscle and liver in this disease,[59,60] then already indicating that the mechanisms of polyglucosan generation in LD are not specific to the brain.

RD is primarily a skeletal and cardiac myopathy, both muscle types showing abundant PBs in patient biopsies or explanted hearts.[13,16] In the absence of autopsies, it is not yet known whether they occur in the brain. In the *Rbck1*$^{-/-}$ mice, PBs have so far been noted only in the heart.[61,62] We analysed 14–16-month-old *Rbck1*$^{-/-}$ mice and discovered the presence of profuse PB accumulation in the CNS, with the highest amounts in the hippocampus, cerebellum and central spinal cord (Fig. 1A–C). Already at 6 months of age the PB load is substantial in the hippocampus and cerebellum (Supplementary Fig. 1A). Total brain glycogen, which comprises normal and PB glycogen, quantified biochemically was significantly increased (Fig. 1D). These results indicate that, like LD and APBD, the amylopectinosis of RD affects the brain.

Rbck1$^{-/-}$ brain glycogen is hyperphosphorylated and long-chained

Glycogen is hyperphosphorylated in LD and not in APBD.[39,57,63–65] We measured phosphorylation at the C6 carbons of glycogen-derived glucose from *Rbck1*$^{-/-}$ brain and found it to be increased like in LD (Fig. 1E). Quantitatively, the elevated C6 phosphate levels are in the range of what is seen in LD.[57]

Glycogen branching insufficiency underlies the generation of overly long glycogen branches in APBD. What causes the same in LD is unknown. One possibility considered was that the laforin–malin complex regulates GYS, and that in its absence GYS outpaces GBE1 to generate overlong branches.[66] This hypothesis was not confirmed as levels and activity of soluble GYS in brain and other tissue extracts of LD mice were found to be normal.[63,67] We now tested this hypothesis in RD. As in LD, soluble GYS levels (Fig. 1F) and activity (Supplementary Fig. 1B and C) in *Rbck1*$^{-/-}$ brain extracts were normal. As in LD,[63,67] total GYS levels were increased (Fig. 1H), but this increase is due to the elevated GYS levels in the insoluble fraction of tissue extracts (Fig. 1G). As documented in LD, only soluble GYS is active and can elongate glycogen branches, and the increased GYS in the insoluble fraction represents protein which, as a glycogen-binding protein, co-precipitates with and is trapped, inactive, in the accumulating polyglucosans.[63,67] Soluble portions of GBE1 and laforin were likewise unaltered and both, like GYS, were accumulated in the insoluble fraction (Fig. 1F and G).

Based on their staining with PASD and their ultrastructural appearance, the abnormal accumulation in RD have been, rightly, concluded to be polyglucosan.[13,15–17] We proceeded to document this formally and measured the actual lengths of glycogen chains. CLD analysis confirmed that *Rbck1*$^{-/-}$ brain glycogen has a deficit of shorter chains and an excess of longer chains (Fig. 1I). This confirms that RD glycogen is in part polyglucosan and the accumulations in RD *bona fide* amylopectinosis.

In summary, similar to APBD and LD, the amylopectinosis of RD includes the brain. Glycogen in RD is similar to that of APBD and LD in encompassing glycogen with overlong branches. The latter is not driven by increased GYS1 levels or activity. Finally, glycogen in RD is similar to that of LD and different from that of APBD in being hyperphosphorylated.

14–16-month-old *Rbck1*$^{-/-}$ mice have apparent cerebellar deficits

We observed that as they reached 14 months of age some *Rbck1*$^{-/-}$ mice started walking clumsily, stumbling as they ambulated. This continued to worsen as they further aged. We proceeded to quantify behavioural deficits. In these experiments we utilized only female mice. We tested the mice for their ability to cross a horizontal beam, balance on a rotating rod and descend from a vertical beam, and measured an index of gait regularity. Results of all of these were abnormal in the *Rbck1*$^{-/-}$ mice compared to those of wild-type female littermates (Fig. 1J–M). We also performed tests of grip strength and exploratory behaviour in an open field. Results of these tests were similar to those of wild-type females (Fig. 1N and O), indicating that female *Rbck1*$^{-/-}$ mice do not exhibit muscle weakness or an obviously decreased activity level. The balance and coordination deficits (crossing a beam, rotarod and descending down a pole) suggest cerebellar involvement, which would be consistent with the particular profusion of PBs in that brain region. Of course, supratentorial, spinal cord, brainstem or neuromuscular contributions to the phenotype cannot be excluded.

Polyglucosan bodies localize mainly in astrocytes and cause neuroinflammation

PBs in LD were reported by Lafora only a few years after his teacher Cajal had developed the Neuron Doctrine of the brain.[58,68] The large majority of brain PBs are in cell processes rather than cell bodies. Lafora and subsequent pathologists for many decades assumed these processes were neuronal, although they did not rule out the astrocytic alternative.[69] Recent studies using co-immunostaining experiments showed that LD PBs are in fact predominantly in astrocytic processes, with a small minority in neurons.[70,71]

To determine the brain cell type in which RD PBs accumulate, we co-immunostained brain sections for markers of astrocytes (GFAP), microglia (IBA1), neurons (TUJ1 and NeuN) and the PBs (GYS). GYS accumulates in PBs and is an established marker for the latter. In immunofluorescence microscopy, signal from GYS molecules present on normal soluble glycogen is as diffuse as glycogen, and practically invisible. When concentrated in PBs, the GYS signal manifests as distinct puncta of different sizes depending on the size of the PB.[47,70,72] We found that the overwhelming majority of PBs in *Rbck1*$^{-/-}$ brain are in astrocytes and their processes (Fig. 2A and Supplementary Video 1), with minimal although not inexistent overlap with the microglial and neuronal markers (Supplementary Fig. 2A–C).

The above and follow-up immunohistochemical studies disclosed the presence of a dramatic astrogliosis and microgliosis in

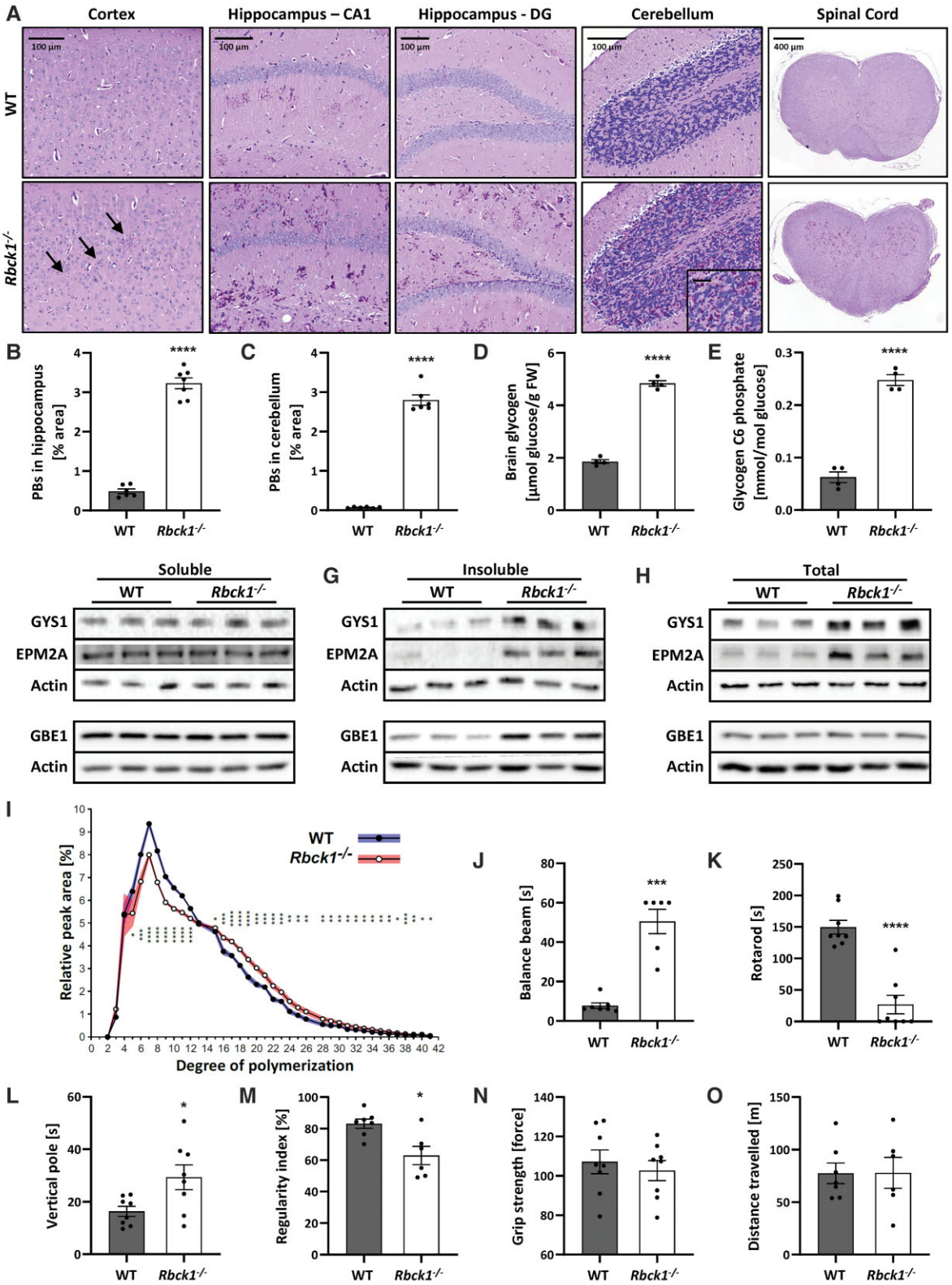

Figure 1 Brain PB disease in *Rbck1*$^{-/-}$ mice is associated with behavioural abnormalities. (**A**) Representative images of PASD-stained cortex, hippocampus, cerebellum and spinal cord of wild-type (WT) versus *Rbck1*$^{-/-}$ mice. (**B** and **C**) PB quantification in the hippocampus (**B**) and cerebellum (**C**). (**D**) Brain total glycogen content in wild-type and *Rbck1*$^{-/-}$ mice. (**E**) Brain glycogen C6 phosphate in wild-type and *Rbck1*$^{-/-}$ mice. (**F**–**H**) Brain western blots against glycogen synthase 1 (GYS1), laforin (EPM2A), glycogen branching enzyme 1 (GBE1) in soluble (**F**), insoluble (**G**) and total lysates (**H**) with actin as loading control. (**I**) Chain length distributions (CLDs) of total brain glycogen from wild-type and *Rbck1*$^{-/-}$ mice. (**J**–**O**) Behavioural testing conducted with wild-type and *Rbck1*$^{-/-}$ mice, including balance beam (**J**), rotarod (**K**), vertical pole (**L**), gait analysis (**M**), grip strength (**N**) and open field (**O**). All data are presented as mean ± SEM (except for SD as shaded area in **I**). Biological replicates $n = 6$–7 (**B** and **C**), $n = 4$ (**D** and **E**), $n = 3$ (**F**–**H**), $n = 4$ (**I**), $n = 6$–8 (**J**–**O**). Significance levels are indicated as $^{*}P < 0.05$; $^{**}P < 0.01$; $^{***}P < 0.001$; $^{****}P < 0.0001$. Mixed sexes were used for all analyses, except behavioural testing where only females were used.

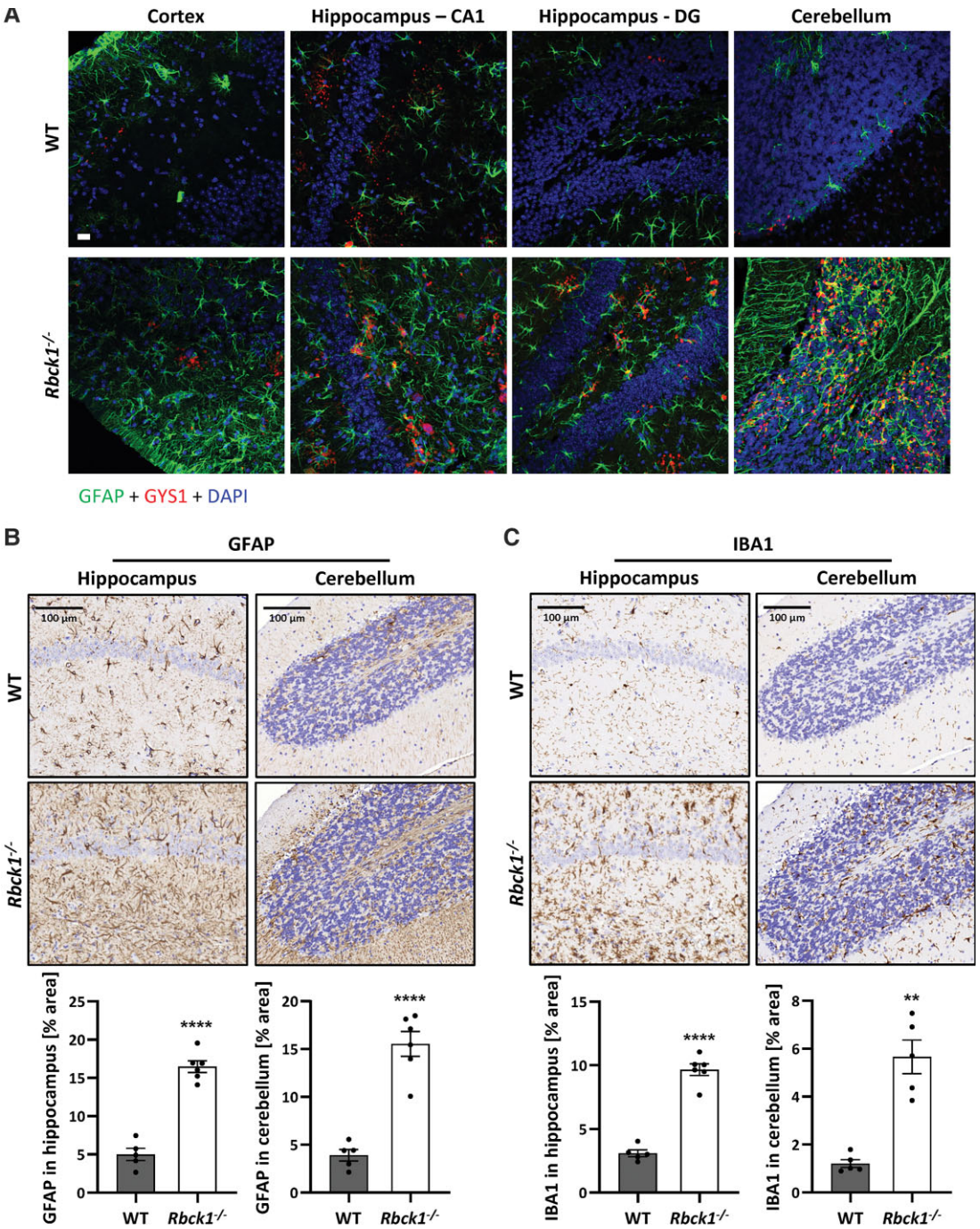

Figure 2 Astrocytic PBs in *Rbck1*$^{-/-}$ mice cause neuroinflammation, both astrogliosis and microgliosis. (**A**) Co-immunostaining against GYS1 for PB detection (red) and the astrocyte marker GFAP (green) showing localization of PBs in astrocytes. Nuclear stain with DAPI (blue). Scale bar = 20 µm. Video compilation of cerebellar confocal z-stack images in Supplementary Video 1. (**B** and **C**) Representative immunohistochemistry (IHC) images with signal quantification of anti-GFAP (**B**) and anti-IBA1 IHCs (**C**) in hippocampus and cerebellum of wild-type (WT) and *Rbck1*$^{-/-}$ mice. All data are presented as mean ± SEM. Biological replicates $n = 5–6$ (**B** and **C**). Significance levels are indicated as $^{**}P < 0.01$; $^{****}P < 0.0001$. Mixed sexes were used.

the *Rbck1*$^{-/-}$ mice (Fig. 2B and C). The extent of this neuroinflammation is similar to what is seen in LD and APBD.[40,44,72]

Polyglucosan bodies in *Rbck1*$^{-/-}$ skeletal and cardiac muscle are sex-specific

Skeletal myopathy is a cardinal feature of RD, yet in the *Rbck1*$^{-/-}$ mice PBs have to date been reported only in the heart.[61] We confirmed their presence in the heart (Fig. 3A) and now also report their presence in large amounts in skeletal muscle (Fig. 3D).

Proceeding to quantify PBs and glycogen in cardiac and skeletal muscles of the *Rbck1*$^{-/-}$ mice, we noted that hearts of female mice had vastly fewer PBs than those of the males (Fig. 3A and B and Supplementary Fig. 3A and B). In skeletal muscle, the contrast seemed even greater. While male *Rbck1*$^{-/-}$ mice had abundant PBs, females had very few (Fig. 3D and E and

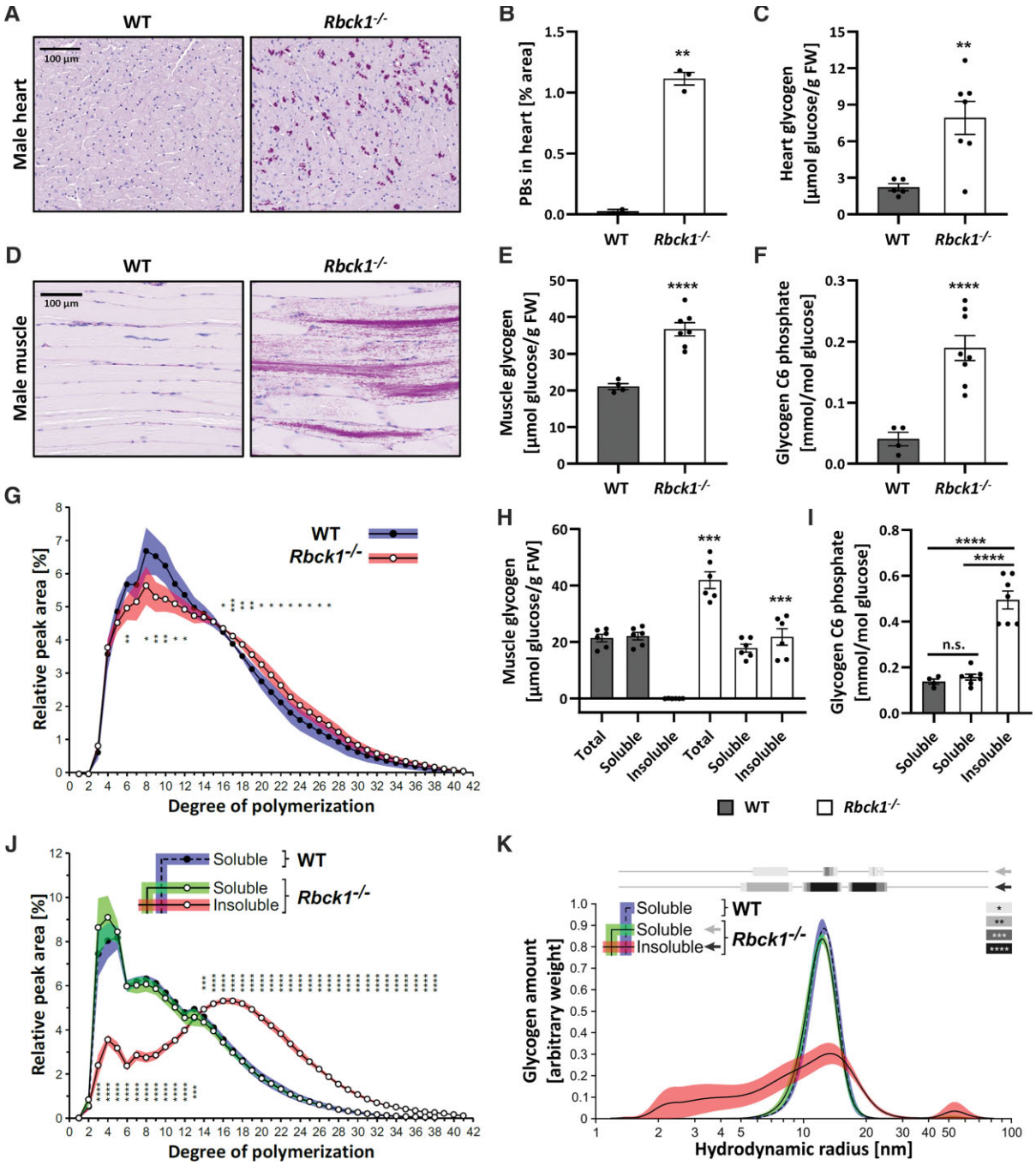

Figure 3 PB accumulation in the heart and skeletal muscle of *Rbck1*$^{-/-}$ mice with insoluble muscle glycogen exhibiting hyperphosphorylation, abnormal chain lengths and molecule sizes. (**A**) Representative images of PASD-stained heart of wild-type (WT) and *Rbck1*$^{-/-}$ mice. (**B**) PB quantification in the heart. (**C**) Total heart glycogen. (**D**) Representative images of PASD-stained skeletal muscle of wild-type versus *Rbck1*$^{-/-}$ mice. (**E**) Total skeletal muscle glycogen. (**F**) Skeletal muscle glycogen C6 phosphate in wild-type and *Rbck1*$^{-/-}$ mice. (**G**) Chain length distributions (CLDs) of total skeletal muscle glycogen from wild-type and *Rbck1*$^{-/-}$ mice. (**H–K**) Glycogen analyses in glycogen fractions from skeletal muscle of wild-type and *Rbck1*$^{-/-}$ mice. Glycogen content in total, soluble and insoluble fractions (**H**) and in selected wild-type and *Rbck1*$^{-/-}$ fractions glycogen C6 phosphate (**I**), CLDs (**J**) and MSDs (**K**). All data are presented as mean ± SEM (except for SD as shaded area in **G**, **J** and **K**). Biological replicates $n = 2–3$ (**B**), $n = 4–8$ (**C**, **E** and **F**), $n = 4$ (**G**), $n = 4–7$ (**H** and **I**), $n = 6$ (**J** and **K**). Significance levels are indicated as $^{*}P < 0.05$; $^{**}P < 0.01$; $^{***}P < 0.001$; $^{****}P < 0.0001$. For statistical analyses in **H**, corresponding fractions in *Rbck1*$^{-/-}$ and wild-type were compared. In **J** and **K**, both *Rbck1*$^{-/-}$ fractions were compared to wild-type. In **K**, statistical significance is displayed by grey-scale bars and arrows indicate which *Rbck1*$^{-/-}$ fraction was used for comparison. Male mice were used for all analyses.

Supplementary Fig. 3D and E). To confirm this observation biochemically, we quantified total glycogen (which, as mentioned, is a sum of normal and PB glycogen) from male and female hearts and skeletal muscle. Male *Rbck1*$^{-/-}$ heart glycogen was increased 3-fold compared to male wild-type heart glycogen (Fig. 3C). In females, *Rbck1*$^{-/-}$ heart glycogen was not increased to a statistically significant degree compared to wild-type (Supplementary Fig. 3C). Male *Rbck1*$^{-/-}$ skeletal muscle glycogen was increased

approximately 2-fold compared to male wild-type skeletal muscle glycogen (Fig. 3E). Female *Rbck1*$^{-/-}$ skeletal muscle glycogen was not increased at all (Supplementary Fig. 3E), consistent with the extremely low numbers of PBs in that tissue in female *Rbck1*$^{-/-}$ mice.

The liver is another major glycogen metabolizing organ. To date, PBs have been reported in one liver biopsy in a patient with RD.[16] We studied the livers of *Rbck1*$^{-/-}$ mice and found no definitive PBs in either sex, and correspondingly no increased glycogen compared to wild-type (Supplementary Fig. 3H and I). This situation is reminiscent of LD, where human patients exhibit PBs in the liver, albeit of no clinical significance, but LD mouse models, even at an advanced age, manifest no definitive PASD-positive inclusions (unpublished observations). The APBD mouse model, on the other hand, does exhibit hepatic PBs.[44]

Rbck1$^{-/-}$ glycogen characteristics recapitulate those of *Epm2b*$^{-/-}$ Lafora disease

As mentioned, laforin is a glycogen phosphatase and glycogen is hyperphosphorylated in LD caused by laforin deficiency (*Epm2a*$^{-/-}$). Muscle contains substantially more glycogen than brain, which allows us to separate PB (insoluble) from soluble glycogen and still obtain sufficient amounts of each to perform the particularly fine measurements needed to quantify glycogen phosphate and determine glycogen CLD.[39] We previously performed these measurements in the mouse models of both forms of LD (*Epm2a*$^{-/-}$ and *Epm2b*$^{-/-}$) and APBD (*Gbe1*$^{ys/ys}$) and found that both normal and PB glycogen are hyperphosphorylated in *Epm2a*$^{-/-}$, only PB glycogen is hyperphosphorylated in *Epm2b*$^{-/-}$ and neither is hyperphosphorylated in *Gbe1*$^{ys/ys}$. The CLD was abnormal only in PB glycogen in all three models.[39]

We now quantified glycogen C6 phosphate and performed CLD analysis on glycogen from skeletal muscle of male and female *Rbck1*$^{-/-}$ mice. Glycogen phosphate was increased (Fig. 3F) and glycogen chains were abnormally long (Fig. 3G) only in male *Rbck1*$^{-/-}$ skeletal muscle glycogen. These two parameters were like wild-type in the female mice (Supplementary Fig. 3F and G). After separating and quantifying PB (insoluble) and normal (soluble) glycogen in muscle of the PB-accumulating males (Fig. 3H), we determined that hyperphosphorylation (Fig. 3I) and glycogen with long branches (Fig. 3J) was only found in the insoluble PB glycogen.

While CLD analysis defines the composition of glycogen chains lengths, we also sought to measure the distribution of whole glycogen molecule sizes (MSD). We previously obtained MSD measurements of soluble and insoluble muscle glycogen from the APBD and LD mouse models.[39] Soluble glycogen in the three models was similar to wild-type with a slight shift towards larger sizes in APBD. Insoluble glycogen differed from wild-type in all three models with an enrichment of small molecules in all three and of large molecules only in the two LD models. Results of MSD analysis of male *Rbck1*$^{-/-}$ muscle glycogen were identical to those of LD (Fig. 3K and Supplementary Fig. 3J).

In summary, *Rbck1*$^{-/-}$ muscle glycogen differs from that of APBD in glycogen phosphorylation and MSD, and from *Epm2a*$^{-/-}$ in hyperphosphorylation limited to PB glycogen. It does not differ from *Epm2b*$^{-/-}$ glycogen in any respect studied.

Partial depletion or deactivation of GYS1 rescues murine RBCK1 deficiency

As seen above, the one constant in PB glycogen across all genetic causes of amylopectinosis studied, now including RD, is the overlong glycogen branches. GYS effectuates chain lengthening and can be downregulated by reducing its quantity or activity. We and others previously partially depleted or deactivated GYS1 (brain and muscle isoform of GYS) in the APBD and LD mouse models through various means. In all cases this resulted in rescue of the disease phenotypes.[40–49] To test if this therapeutic strategy is also applicable to RD, we generated two genetic models: one, *Rbck1*$^{-/-}$ mice with mono-allelic knockout of *Gys1* (*Rbck1*$^{-/-}$ *Gys1*$^{+/-}$) and the other, *Rbck1*$^{-/-}$ mice with bi-allelic knockout of *Ppp1r3c* (*Rbck1*$^{-/-}$ *Ppp1r3c*$^{-/-}$). *Gys1*$^{+/-}$ reduces GYS1 levels by 50% without affecting its activation state (Supplementary Fig. 4),[73] whereas *Ppp1r3c*$^{-/-}$ reduces GYS1's activation state by ≈25% without significantly affecting GYS1 quantity (Supplementary Fig. 4).[45] Both approaches largely or completely prevented PB formation and glycogen accumulation irrespective of sex in heart (Fig. 4A–D and Supplementary Fig. 5A–D), skeletal muscle (Fig. 4E–G, I and Supplementary Fig. 5E–H) and brain (Fig. 5A–H); corrected the glycogen hyperphosphorylation (Fig. 4H and J); and rescued the astrogliosis (Fig. 6A–D) and microgliosis (Fig. 7A–D). Finally, the behavioural phenotypes observed in female *Rbck1*$^{-/-}$ mice (Fig. 1J–M) were rescued by the 50% depletion of GYS1 (*Rbck1*$^{-/-}$ *Gys1*$^{+/-}$; Fig. 7E–J).

In the experiments toward generating the *Rbck1*$^{-/-}$ *Ppp1r3c*$^{-/-}$ mice, the behavioural phenotypes of the *Rbck1*$^{-/-}$ females disappeared in the process of the various crosses to obtain the experimental and control groups. In other words, due to unknown background genetic factors there no longer was a behavioural phenotype to correct (Fig. 7K–P). We probed our neuropathology data for an explanation for this and noted the following. The *Rbck1*$^{-/-}$ mice from the *Rbck1*$^{-/-}$ *Ppp1r3c*$^{-/-}$ line in fact show little to no cerebellar astrogliosis (Fig. 6B and D) and low levels of cerebellar microgliosis (Fig. 7B and D) compared with *Rbck1*$^{-/-}$ mice from the *Rbck1*$^{-/-}$ *Gys1*$^{+/-}$ line (Figs 6A, C and 7A and C). This could at least in part explain the missing behavioural phenotypes (balance beam, rotarod and gait regularity; Fig. 7K–P), which, as mentioned, are likely heavily cerebellar in origin. The genetics of this peculiar cerebellar specific anti-inflammatory effect awaits future exploration.

We originally limited the behavioural studies to one sex, female, for experimental uniformity. Having observed the sex-based differences in skeletal and cardiac pathology, we revisited the brain and performed behavioural analyses in males of the *Rbck1*$^{-/-}$ *Ppp1r3c*$^{-/-}$ and *Rbck1*$^{-/-}$ *Gys1*$^{+/-}$ lines. Interestingly, the obvious ataxic gait that the females develop as they age was not present in males from either line. Formal testing likewise showed that the males from neither line had the behavioural phenotypes present in the females of the *Rbck1*$^{-/-}$ or *Rbck1*$^{-/-}$ *Gys1*$^{+/-}$ lines (Supplementary Fig. 6A–L). Quantitation of PBs, accumulated glycogen and neuroinflammation showed no differences between male and female littermates of either line (Supplementary Fig. 7A–F). Close pathological analysis revealed one striking difference. In the cochlear nuclei, female *Rbck1*$^{-/-}$ mice with behavioural phenotypes exhibited particularly large PBs associated with vacuolation, the latter feature not seen elsewhere in the brain. Males also had these large PBs in this brain region, but with little to no vacuolation (Supplementary Fig. 7G). The significance of this brain region and sex-specific vacuolar effect awaits future study.

Gys1-targeting ASO rescues the RBCK1 deficient brain amylopectinosis

Toward a GYS1 downregulation-based therapy for LD, we previously developed multiple murine ASOs that effectively decrease *Gys1* mRNA levels and, where tested in LD mice, rescue the LD phenotype.[49] These ASOs have chemistries formulated for CSF delivery

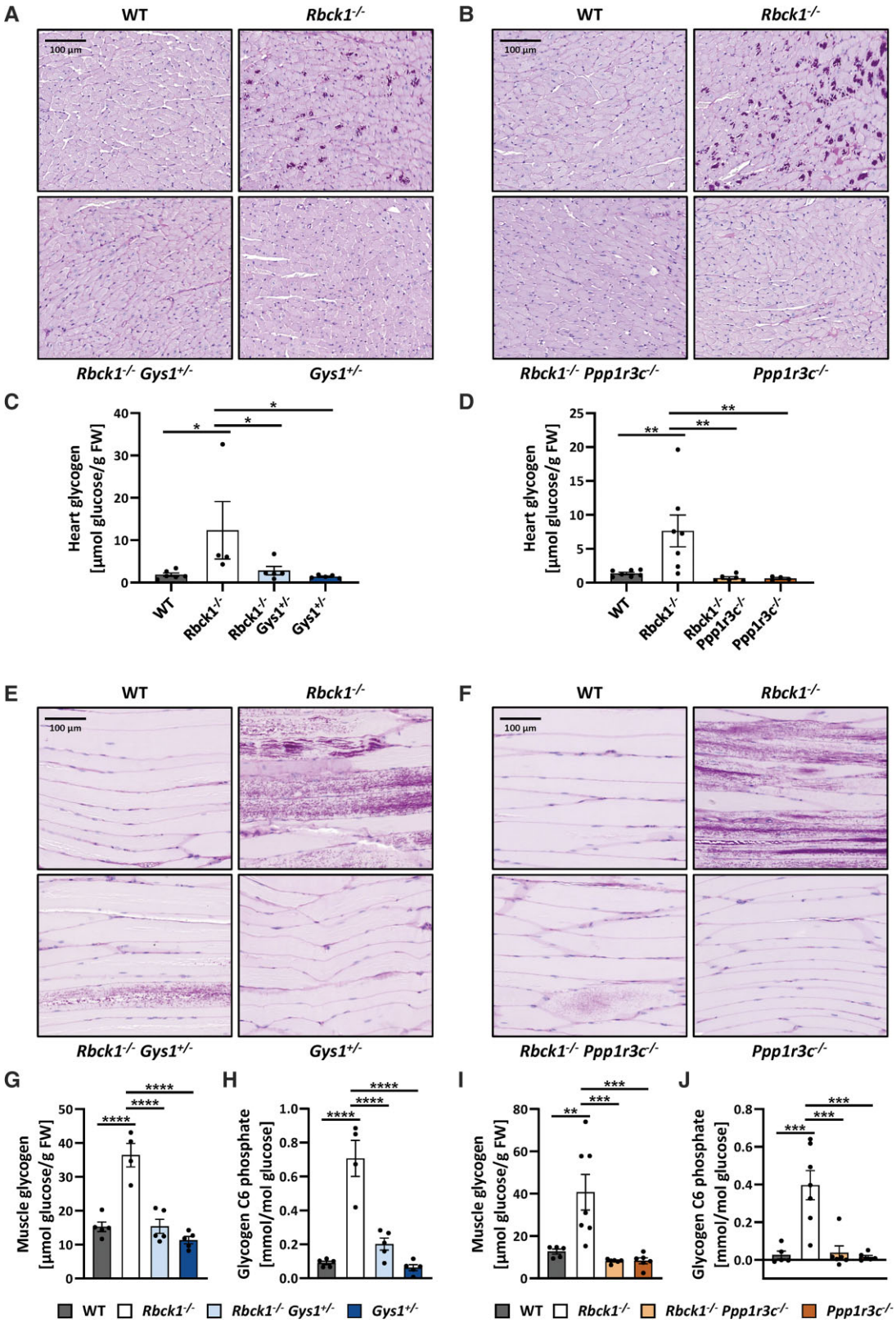

Figure 4 Prevention of PB formation in heart and skeletal muscle of *Rbck1*$^{-/-}$ mice by mono-allelic *Gys1* and bi-allelic *Ppp1r3c* knockout. (**A** and **B**) Representative images of PASD-stained heart from all four genotypes from the *Rbck1*$^{-/-}$ *Gys1*$^{+/-}$ (**A**) and *Rbck1*$^{-/-}$ *Ppp1r3c*$^{-/-}$ line (**B**). (**C** and **D**) Total heart glycogen in all four genotypes from the *Rbck1*$^{-/-}$ *Gys1*$^{+/-}$ (**C**) and *Rbck1*$^{-/-}$ *Ppp1r3c*$^{-/-}$ line (**D**). (**E** and **F**) Representative images of PASD-stained skeletal muscle from all four genotypes from the *Rbck1*$^{-/-}$ *Gys1*$^{+/-}$ (**E**) and *Rbck1*$^{-/-}$ *Ppp1r3c*$^{-/-}$ line (**F**). (**G** and **H**) Total glycogen (**G**) and glycogen C6 phosphate (**H**) in skeletal muscle of all four genotypes from the *Rbck1*$^{-/-}$ *Gys1*$^{+/-}$ line. (**I** and **J**) Total glycogen (**I**) and glycogen C6 phosphate (**J**) in skeletal muscle of all four genotypes from the *Rbck1*$^{-/-}$ *Ppp1r3c*$^{-/-}$ line. All data are presented as mean ± SEM. Biological replicates $n = 4$–7 (**C**, **D** and **G**–**J**). Significance levels are indicated as $^{*}P < 0.05$; $^{**}P < 0.01$; $^{***}P < 0.001$; $^{****}P < 0.0001$. Male mice were used for all analyses. WT = wild-type.

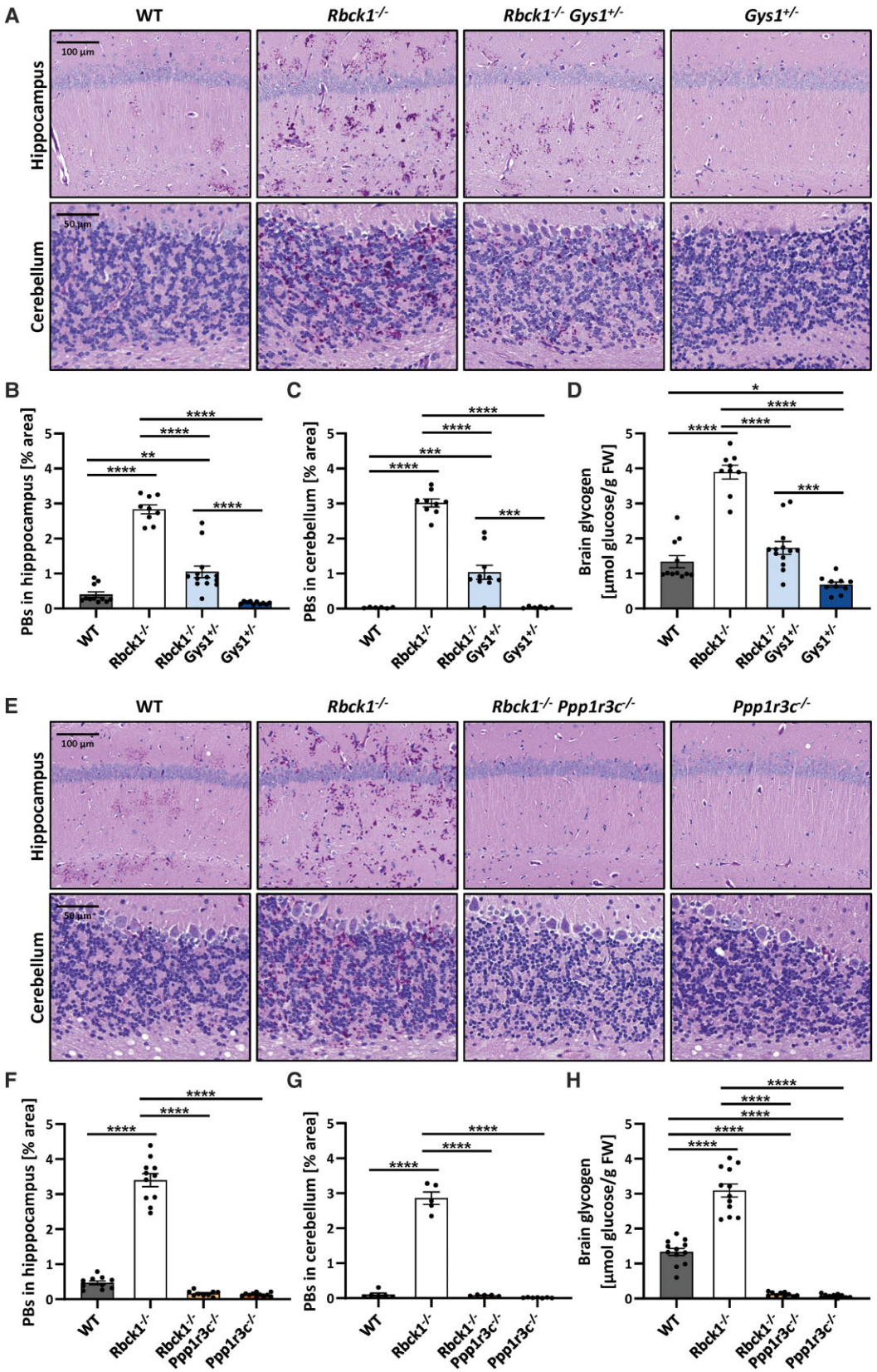

Figure 5 Prevention of PB formation in the brain of *Rbck1*$^{-/-}$ mice by mono-allelic *Gys1* and bi-allelic *Ppp1r3c* knockout. (**A**) Representative images of PASD-stained brain from all four genotypes from the *Rbck1*$^{-/-}$ *Gys1*$^{+/-}$ line. (**B**–**D**) PB quantification in the hippocampus (**B**) and cerebellum (**C**) as well as brain total glycogen (**D**) in all four genotypes from the *Rbck1*$^{-/-}$ *Gys1*$^{+/-}$ line. (**E**) Representative images of PASD-stained brain from all four genotypes from the *Rbck1*$^{-/-}$ *Ppp1r3c*$^{-/-}$ line. (**F**–**H**) PB quantification in the hippocampus (**F**) and cerebellum (**G**) as well as brain total glycogen (**H**) in all four genotypes from the *Rbck1*$^{-/-}$ *Ppp1r3c*$^{-/-}$ line. All data are presented as mean ± SEM. Biological replicates $n = 9$–13 (**B**, **D**, **F** and **H**), $n = 5$–10 (**C** and **G**). Significance levels are indicated as $^{*}P < 0.05$; $^{**}P < 0.01$; $^{***}P < 0.001$; $^{****}P < 0.0001$. Mixed sexes were used. WT = wild-type.

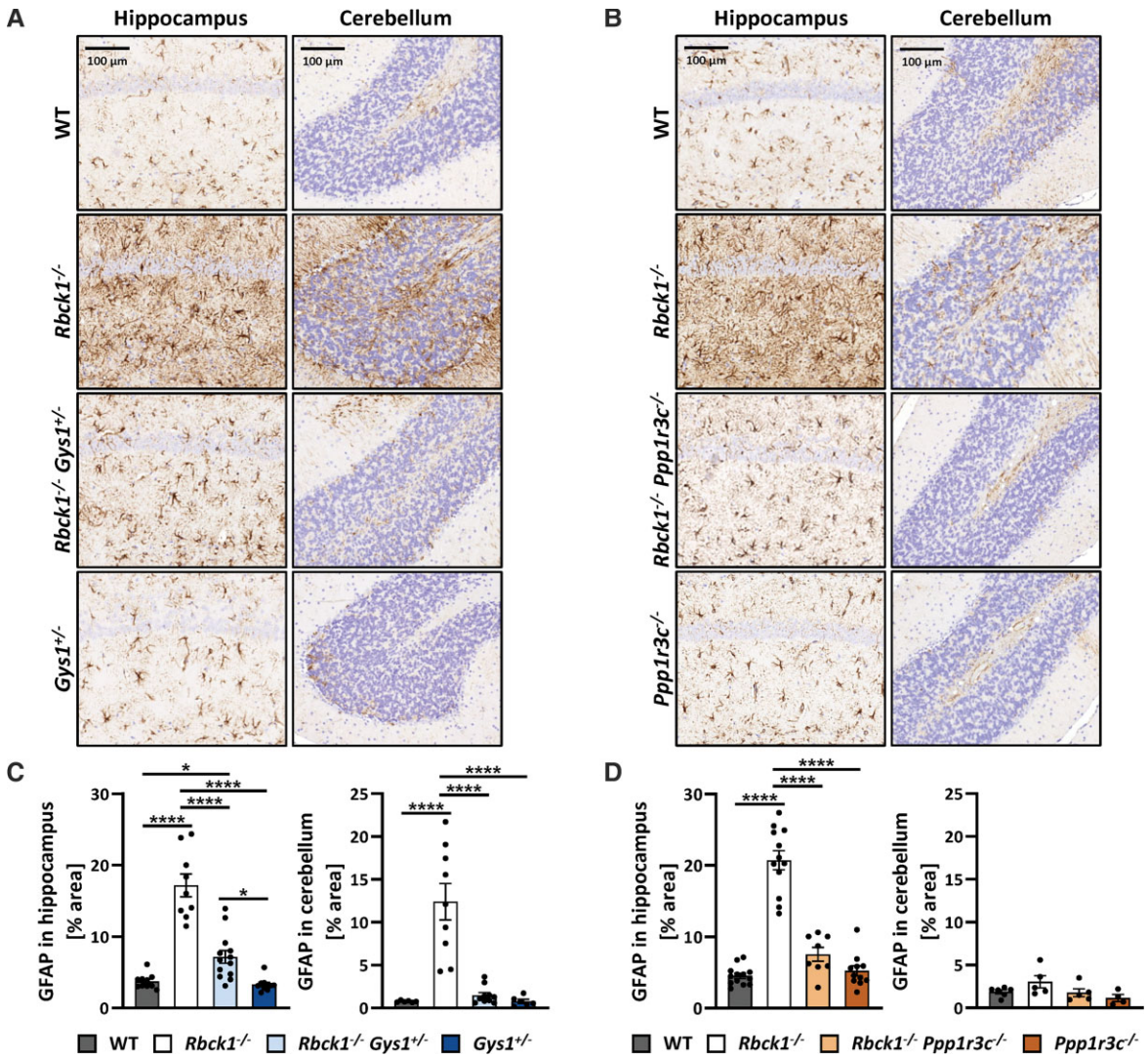

Figure 6 Downregulation of GYS1 via *Gys1* or *Ppp1r3c* knockout rescues astrogliosis in *Rbck1*$^{-/-}$ mice. (**A** and **B**) Representative GFAP IHC images of hippocampus and cerebellum from all four genotypes from the *Rbck1*$^{-/-}$ *Gys1*$^{+/-}$ (**A**) and *Rbck1*$^{-/-}$ *Ppp1r3c*$^{-/-}$ line (**B**). (**C** and **D**) GFAP signal quantification in hippocampus and cerebellum in all four genotypes from the *Rbck1*$^{-/-}$ *Gys1*$^{+/-}$ (**C**) and *Rbck1*$^{-/-}$ *Ppp1r3c*$^{-/-}$ (**D**) line. All data are presented as mean ± SEM. Biological replicates $n = 7$–13 (**C**), $n = 4$–13 (**D**). Significance levels are indicated as $^{*}P < 0.05$; $^{****}P < 0.0001$. Mixed sexes were used for GFAP IHC. WT = wild-type.

and CNS functionality. As a pilot experiment, we used one of them to treat *Rbck1*$^{-/-}$ mice. We injected the mice intracerebroventrically at 1 and 2 months of age and sacrificed them at 3 months. Baseline mice were uninjected 1-month-old mice that served as a reference, as no PBs are detectable at this young age in RD (like in LD). Gys1-ASO treatment reduced brain *Gys1* mRNA (Fig. 8A), led to major reduction in glycogen levels (Fig. 8B) and completely prevented PB formation in *Rbck1*$^{-/-}$ mice (Fig. 8C and D).

Discussion

Glycogen occupies a critical evolutionary niche, namely a large 'in-house' energy store for every individual cell. Maintaining this largest cytosolic molecule in solution is thought to only require balanced GYS and GBE1 activities. However, LD has long challenged this notion. Laforin is a glycogen phosphatase,[10,11] but it was shown that glycogen hyperphosphorylation *per se* does not lead to the acquisition of long chains nor to precipitation.[57,74] Instead, evidence suggests that laforin acts via its interacting partner malin to prevent appearance and accumulation of long-chained insoluble glycogen.[3,57,75] Malin is an E3 ubiquitin ligase whose genuine substrate has so far proven elusive. RD is a more recent challenge to the basic model of glycogen structural integrity. We now show that in every detail tested RD glycogen recapitulates malin-deficient LD glycogen. As such, RD represents a new entryway to the unknown mechanisms of glycogen architecture. RBCK1 is also an E3 ubiquitin ligase. It was recently reported that its glycogen-relevant substrate may be glycogen itself.[33] This raises the possibility that malin's substrate may also be glycogen. Glycogen chains were recently shown to include significant amounts of glucosamines and that in LD these accumulate with polyglucosans.[76] Malin may ubiquitinate glycogen at these amines. The steps beyond glycogen ubiquitination by RBCK1, and potentially malin, would need to be solved. One proposed hypothesis for RBCK1 is that ubiquitination of glycogen activates autophagy to eliminate polyglucosans as they form.[33] It should be

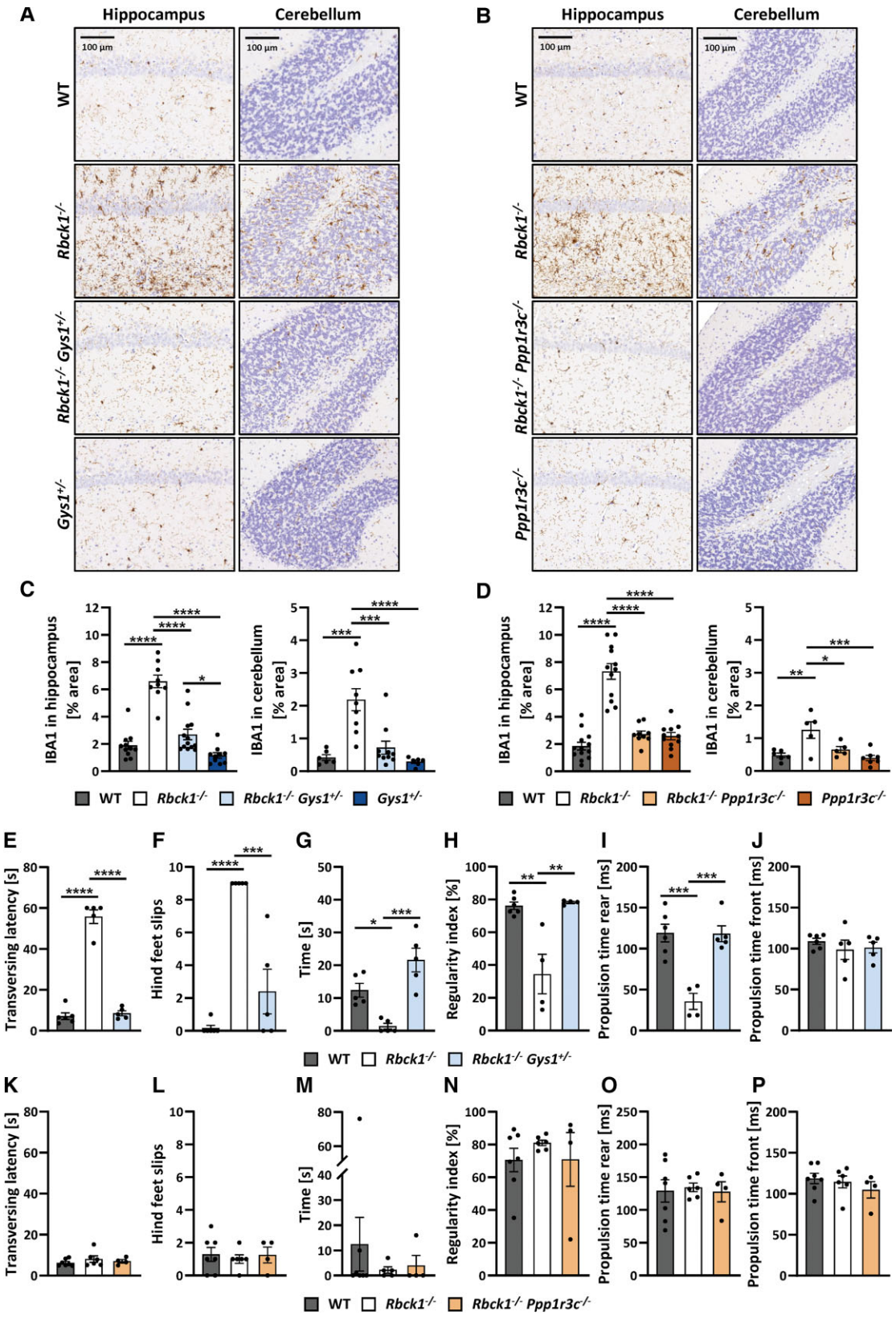

Figure 7 Downregulation of GYS1 rescues microgliosis and behavioural abnormalities in *Rbck1*$^{-/-}$ mice. (**A** and **B**) Representative IBA1 IHC images of hippocampus and cerebellum from all four genotypes from the *Rbck1*$^{-/-}$ *Gys1*$^{+/-}$ (**A**) and *Rbck1*$^{-/-}$ *Ppp1r3c*$^{-/-}$ line (**B**). (**C** and **D**) IBA1 signal quantification in hippocampus and cerebellum in all four genotypes from the *Rbck1*$^{-/-}$ *Gys1*$^{+/-}$ (**C**) and *Rbck1*$^{-/-}$ *Ppp1r3c*$^{-/-}$ (**D**) line. Behavioural testing conducted with wild-type (WT), *Rbck1*$^{-/-}$ and *Rbck1*$^{-/-}$ *Gys1*$^{+/-}$ mice (**E–J**) as well as with WT, *Rbck1*$^{-/-}$ and *Rbck1*$^{-/-}$ *Ppp1r3c*$^{-/-}$ (**K–P**): transversing latency (**E** and **K**) and hind feet slips (**F** and **L**) from balance beam testing, latency to fall from rotarod testing (**G** and **M**) and regularity index (**H** and **N**), rear (**I** and **O**) and front (**J** and **P**) leg propulsion time from gait analysis. All data are presented as mean ± SEM. Biological replicates $n = 6–13$ (**C**), $n = 5–13$ (**D**), $n = 4–7$ (**E–P**). Significance levels are indicated as $^{*}P < 0.05$; $^{**}P < 0.01$; $^{***}P < 0.001$; $^{****}P < 0.0001$. Females were used for behavioural testing, mixed sexes for IBA1 IHC.

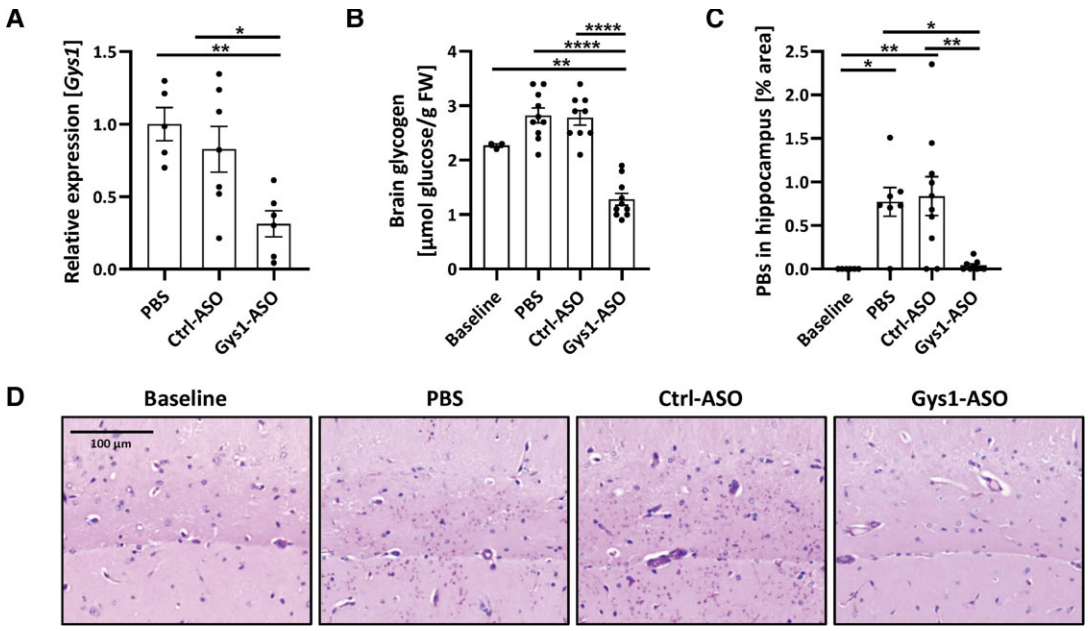

Figure 8 *Gys1*-targeting ASO, administered at 1 and 2 months, leads to reduced *Gys1* mRNA and glycogen levels, and prevents PB accumulation in the brain of *Rbck1*$^{-/-}$ mice at 3 months. PBS, Ctrl-ASO (no-target control ASO), or Gys1-ASO were injected at 1 and 2 months and brain tissue analysed at 3 months. (**A**) Brain *Gys1* mRNA relative expression levels in PBS-, Ctrl-ASO, and Gys1-ASO-injected *Rbck1*$^{-/-}$ mice. (**B**) Brain total glycogen content. (**C**) PB quantification in the hippocampus. (**D**) Representative images of PASD-stained hippocampus. Untreated mice, sacrificed and analysed at 1 month, served as baseline control. All data are presented as mean ± SEM. Biological replicates $n = 3$–10 (**A**–**C**). Significance levels are indicated as $^{*}P < 0.05$; $^{**}P < 0.01$; $^{****}P < 0.0001$. Mixed sexes were used.

noted that ubiquitin was shown to be associated with PBs both in the absence of malin and of RBCK1.[36–38] Whether the ubiquitin association with PBs is through covalent linkages and has a role in PB accumulation is unknown.

Central to immunity is its extremely tight control. The microbial threat is so diverse that unless the response is fine-tuned, collateral damage ensues. The defensive potential is as diverse as the threat, including against molecules and membranes that closely resemble the host's. Even partial, unprovoked unleashing of the immune system will damage the host. This regulation involves a large number of de-ubiquitinating and ubiquitinating enzymes including LUBAC.[77,78] While all patients with RD have amylopectinosis, some also have a significant immune dysregulation and frequent and unusual infections accompanied with autoimmunity.[16,17] These patients often die in early childhood. The genotype–phenotype correlation with the immune dysregulation is complex. There is a trend towards having it with mutations that disrupt RBCK1's N-terminal UBL domain, which would lead to LUBAC destabilization.[17] However, multiple patients have truncating mutations in the central part of the gene, distant from both termini. The *RBCK1* mRNA in these patients is expected to degenerate by NMD and eliminate the UBL. However, these patients do not have the severe immune disease.[13,16] The murine mutations may inform on this paradox. Likely, the process evolved in mouse to preserve RBCK1's N-terminus against the effects of NMD (see *Rbck1*$^{-/-}$ mouse line description in the 'Materials and methods' section)[24] is also operational in humans, thus sparing patients with downstream truncating mutations from the severe immune disease. There is, however, evidence that many patients have some degree of immune disturbance,[16] which is highly variable, e.g. inflammatory bowel disease, synovial inflammation, sarcoidosis, etc. This variation is likely influenced by background genetics. This again is like the mouse. The *Rbck1*$^{-/-}$ mice used here with greatly reduced, but not eliminated, LUBAC do not have significant immune disease but do have susceptibilities to infection by very particular pathogens.[61] In our work here on the brain, we find that the neuroimmunopathology that follows the amylopectinosis is influenced by sex and unknown background genetic influences. This situation is unlike LD and APBD where the neuroimmunopathology is constant. Studies in RD may thus help identify the links between amylopectinosis and inflammation. RD is predominantly a skeletal and cardiac myopathy, but a number of patients do have a variety of neurological symptoms, ranging from seizures to autism and developmental delay.[16,79] One wonders whether the relatively limited and varied neurological presentation is again modulated by the irregular immune dysregulation in this particular disease.

An initial observation we made distinguishing brain pathology in female *Rbck1*$^{-/-}$ mice from their male counterparts is the presence in females of vacuolation around large PBs. The causes of this and their sex dependence need investigation. However, the observation is noteworthy also in that vacuolation around large PBs has been reported in human RD skeletal muscle biopsies.[16] This type of PB-related vacuolation is not seen in LD and APBD. Now captured in a different tissue in a second species, this appears to be an RD-specific phenotype deserving elucidation in the understanding of the disease.

The story of the unknown mechanisms ensuring glycogen structural adequacy is unlikely to end with the uncovering of the laforin–malin–LUBAC intersecting pathways. Very recently, yet another PB disease was described. Here again the function of the identified disease gene product, KLHL24, is not known, except that it is a substrate-specific adaptor for a class (cullin E3) of E3 ubiquitin ligases.[80]

A potential treatment for the various amylopectinoses does not need to await the elucidation of the laforin–malin–LUBAC pathways. It is sufficiently clear that the shared pathogenic event is the formation of overly long glycogen chains driving glycogen to precipitation. With our present results, RD, like APBD and both forms

of LD, can be rescued by GYS downregulation. This downregulation can be in quantity or activity. The latter appears to be more effective as relative (≈25%) deactivation of GYS1 with *Ppp1r3c*$^{-/-}$ more completely removed PBs than partial (≈50%) depletion of GYS1 with *Gys1*$^{+/-}$ (*cf*. Fig. 5A–C with Fig. 5E–G). This apparent advantage of deactivation over depletion may contain pathogenic meaning. Possibly, polyglucosan formation is more likely with more active GYS outpacing GBE1, versus more abundant GYS. Notwithstanding, both depletion and deactivation effectively reduce PBs and attendant neuroinflammation. There are presently a number of GYS downregulating pharmacotherapies being developed for LD and APBD, including small molecule inhibitors of GYS1[81] and an ASO against its RNA.[49] The present study suggests that these drugs may be purposed also for RD, especially its fatal cardiac disease and disabling skeletal myopathy.

Acknowledgements

We would like to thank Igor Vukobradovic at The Centre for Phenogenomics for help with behavioural testing; Drs. Michael Emes and Ian Tetlow (University of Guelph, Canada) and Dr Jennifer Kohler (UT Southwestern Medical Center, United States) for access to their HPAEC-PAD equipment; and personnel of the UT Southwestern Live Cell Imaging Facility, a Shared Resource of the Harold C. Simmons Cancer Center, supported in part by the NCI Cancer Center Support Grant 1P30 CA142543-01.

Funding

This work was funded by the National Institute of Neurological Disorders and Stroke under award number P01NS097197. M.A.S. was supported by National Health and Medical Research Council CJ Martin (GNT1092451) and Advance Queensland Industry Research Fellowship and the Mater Foundation, Equity and the L G McCallam Est and George Weaber Trusts. S.A. was supported by the Sigrid Jusélius Foundation. B.A.M. holds the UT Southwestern Jimmy Elizabeth Westcott Chair in Pediatric Neurology.

Competing interests

H.K. is a shareholder and employee at Ionis pharmaceuticals. T.R.G. has a patent (16/306831) pending. Other authors report no competing interests.

Supplementary material

Supplementary material are available at *Brain* online.

References

1. Gidley MJ, Bulpin PV. Crystallisation of malto-oligosaccharides as models of the crystalline forms of starch: Minimum chain-length requirement for the formation of double helices. *Carbohydr Res*. 1987;161(2):291–300.
2. Roach PJ, Depaoli-Roach AA, Hurley TD, Tagliabracci VS. Glycogen and its metabolism: Some new developments and old themes. *Biochem J*. 2012;441:763–787.
3. Nitschke F, Ahonen SJ, Nitschke S, Mitra S, Minassian BA. Lafora disease—From pathogenesis to treatment strategies. *Nat Rev Neurol*. 2018;14(10):606–617.
4. Robitaille Y, Carpenter S, Karpati G, DiMauro SD. A distinct form of adult polyglucosan body disease with massive involvement of central and peripheral neuronal processes and astrocytes: A report of four cases and a review of the occurrence of polyglucosan bodies in other conditions such as Lafora's disease and normal ageing. *Brain*. 1980;103(2):315–336.
5. Lossos A, Meiner Z, Barash V, *et al*. Adult polyglucosan body disease in Ashkenazi Jewish patients carrying the Tyr329Ser mutation in the glycogen-branching enzyme gene. *Ann Neurol*. 1998;44(6):867–872.
6. Akman HO, Kakhlon O, Coku J, *et al*. Deep intronic GBE1 mutation in manifesting heterozygous patients with adult polyglucosan body disease. *JAMA Neurol*. 2015;72(4):441–445.
7. Souza PVS, Badia BML, Farias IB, *et al*. GBE1-related disorders: Adult polyglucosan body disease and its neuromuscular phenotypes. *J Inherit Metab Dis*. 2021;44(3):534–543.
8. Minassian BA, Lee JR, Herbrick JA, *et al*. Mutations in a gene encoding a novel protein tyrosine phosphatase cause progressive myoclonus epilepsy. *Nat Genet*. 1998;20(2):171–174.
9. Chan EM, Bulman DE, Paterson AD, *et al*. Genetic mapping of a new Lafora progressive myoclonus epilepsy locus (EPM2B) on 6p22. *J Med Genet*. 2003;40(9):671–675.
10. Worby CA, Gentry MS, Dixon JE. Laforin, a dual specificity phosphatase that dephosphorylates complex carbohydrates. *J Biol Chem*. 2006;281(41):30412–30418.
11. Tagliabracci VS, Turnbull J, Wang W, *et al*. Laforin is a glycogen phosphatase, deficiency of which leads to elevated phosphorylation of glycogen *in vivo*. *Proc Natl Acad Sci USA*. 2007;104(49):19262–19266.
12. Gentry MS, Worby CA, Dixon JE. Insights into Lafora disease: Malin is an E3 ubiquitin ligase that ubiquitinates and promotes the degradation of laforin. *Proc Natl Acad Sci U S A*. 2005;102(24):8501–8506.
13. Nilsson J, Schoser B, Laforet P, *et al*. Polyglucosan body myopathy caused by defective ubiquitin ligase RBCK1. *Ann Neurol*. 2013;74(6):914–919.
14. Wang K, Kim C, Bradfield J, *et al*. Whole-genome DNA/RNA sequencing identifies truncating mutations in RBCK1 in a novel Mendelian disease with neuromuscular and cardiac involvement. *Genome Med*. 2013;5(7):67.
15. Krenn M, Salzer E, Simonitsch-Klupp I, *et al*. Mutations outside the N-terminal part of RBCK1 may cause polyglucosan body myopathy with immunological dysfunction: Expanding the genotype–phenotype spectrum. *J Neurol*. 2018;265(2):394–401.
16. Phadke R, Hedberg-Oldfors C, Scalco RS, *et al*. RBCK1-related disease: A rare multisystem disorder with polyglucosan storage, auto-inflammation, recurrent infections, skeletal, and cardiac myopathy—Four additional patients and a review of the current literature. *J Inherit Metab Dis*. 2020;43(5):1002–1013.
17. Boisson B, Laplantine E, Prando C, *et al*. Immunodeficiency, autoinflammation and amylopectinosis in humans with inherited HOIL-1 and LUBAC deficiency. *Nat Immunol*. 2012;13(12):1178–1186.
18. Kirisako T, Kamei K, Murata S, *et al*. A ubiquitin ligase complex assembles linear polyubiquitin chains. *EMBO J*. 2006;25(20):4877–4887.
19. Gerlach B, Cordier SM, Schmukle AC, *et al*. Linear ubiquitination prevents inflammation and regulates immune signalling. *Nature*. 2011;471(7340):591–596.
20. Ikeda F, Deribe YL, Skanland SS, *et al*. SHARPIN forms a linear ubiquitin ligase complex regulating NF-kappaB activity and apoptosis. *Nature*. 2011;471(7340):637–641.
21. Tokunaga F, Nakagawa T, Nakahara M, *et al*. SHARPIN is a component of the NF-kappaB-activating linear ubiquitin chain assembly complex. *Nature*. 2011;471(7340):633–636.

22. Stieglitz B, Morris-Davies AC, Koliopoulos MG, Christodoulou E, Rittinger K. LUBAC synthesizes linear ubiquitin chains via a thioester intermediate. *EMBO Rep*. 2012;13(9):840–846.
23. Yagi H, Ishimoto K, Hiromoto T, *et al*. A non-canonical UBA–UBL interaction forms the linear-ubiquitin-chain assembly complex. *EMBO Rep*. 2012;13(5):462–468.
24. Fujita H, Tokunaga A, Shimizu S, *et al*. Cooperative domain formation by homologous motifs in HOIL-1L and SHARPIN plays a crucial role in LUBAC stabilization. *Cell Rep*. 2018;23(4):1192–1204.
25. Iwai K, Fujita H, Sasaki Y. Linear ubiquitin chains: NF-kappaB signalling, cell death and beyond. *Nat Rev Mol Cell Biol*. 2014; 15(8):503–508.
26. Aboujaoude A, Minassian B, Mitra S. LUBAC: A new player in polyglucosan body disease. *Biochem Soc Trans*. 2021;49:2443–2454.
27. Iwai K. LUBAC-mediated linear ubiquitination: A crucial regulator of immune signaling. *Proc Jpn Acad Ser B Phys Biol Sci*. 2021; 97(3):120–133.
28. Fuseya Y, Fujita H, Kim M, *et al*. The HOIL-1L ligase modulates immune signalling and cell death *via* monoubiquitination of LUBAC. *Nat Cell Biol*. 2020;22(6):663–673.
29. Smit JJ, van Dijk WJ, El Atmioui D, Merkx R, Ovaa H, Sixma TK. Target specificity of the E3 ligase LUBAC for ubiquitin and NEMO relies on different minimal requirements. *J Biol Chem*. 2013;288(44):31728–31737.
30. Carvajal AR, Grishkovskaya I, Gomez Diaz C, *et al*. The linear ubiquitin chain assembly complex (LUBAC) generates heterotypic ubiquitin chains. *eLife*. 2021;10:e60660.
31. Kelsall IR, Zhang J, Knebel A, Arthur JSC, Cohen P. The E3 ligase HOIL-1 catalyses ester bond formation between ubiquitin and components of the Myddosome in mammalian cells. *Proc Natl Acad Sci USA*. 2019;116(27):13293–13298.
32. Cohen P, Kelsall IR, Nanda SK, Zhang J. HOIL-1, an atypical E3 ligase that controls MyD88 signalling by forming ester bonds between ubiquitin and components of the Myddosome. *Adv Biol Regul*. 2020;75:100666.
33. Kelsall IR, McCrory EH, Xu Y, *et al*. HOIL-1-catalysed ubiquitylation of unbranched glucosaccharides and its activation by ubiquitin oligomers. bioRxiv, 2021:2021.09.10.459791.
34. Ganesh S, Delgado-Escueta AV, Sakamoto T, *et al*. Targeted disruption of the Epm2a gene causes formation of Lafora inclusion bodies, neurodegeneration, ataxia, myoclonus epilepsy and impaired behavioral response in mice. *Hum Mol Genet*. 2002;11(11): 1251–1262.
35. Lohi H, Ianzano L, Zhao XC, *et al*. Novel glycogen synthase kinase 3 and ubiquitination pathways in progressive myoclonus epilepsy. *Hum Mol Genet*. 2005;14(18):2727–2736.
36. Criado O, Aguado C, Gayarre J, *et al*. Lafora bodies and neurological defects in malin-deficient mice correlate with impaired autophagy. *Hum Mol Genet*. 2012;21(7):1521–1533.
37. Chambers JK, Thongtharb A, Shiga T, *et al*. Accumulation of laforin and other related proteins in canine lafora disease with EPM2B repeat expansion. *Vet Pathol*. 2018;55(4):543–551.
38. Thomsen C, Malfatti E, Jovanovic A, *et al*. Proteomic characterisation of polyglucosan bodies in skeletal muscle in RBCK1 deficiency. *Neuropathol Appl Neurobiol*. 2022;48(1):e12761.
39. Sullivan MA, Nitschke S, Skwara EP, *et al*. Skeletal muscle glycogen chain length correlates with insolubility in mouse models of polyglucosan-associated neurodegenerative diseases. *Cell Rep*. 2019;27(5):1334–1344.e6.
40. Turnbull J, DePaoli-Roach AA, Zhao X, *et al*. PTG depletion removes Lafora bodies and rescues the fatal epilepsy of Lafora disease. *PLoS Genet*. 2011;7(4):e1002037.
41. Pederson BA, Turnbull J, Epp JR, *et al*. Inhibiting glycogen synthesis prevents lafora disease in a mouse model. *Ann Neurol*. 2013;74(2):297–300.
42. Turnbull J, Epp JR, Goldsmith D, *et al*. PTG protein depletion rescues malin-deficient Lafora disease in mouse. *Ann Neurol*. 2014; 75(3):442–446.
43. Duran J, Gruart A, Garcia-Rocha M, Delgado-Garcia JM, Guinovart JJ. Glycogen accumulation underlies neurodegeneration and autophagy impairment in Lafora disease. *Hum Mol Genet*. 2014; 23(12):3147–3156.
44. Chown EE, Wang P, Zhao X, *et al*. GYS1 or PPP1R3C deficiency rescues murine adult polyglucosan body disease. *Ann Clin Transl Neurol*. 2020;7(11):2186–2198.
45. Israelian L, Nitschke S, Wang P, *et al*. Ppp1r3d deficiency preferentially inhibits neuronal and cardiac Lafora body formation in a mouse model of the fatal epilepsy Lafora disease. *J Neurochem*. 2020;157:1897–1910.
46. Nitschke S, Chown EE, Zhao X, *et al*. An inducible glycogen synthase-1 knockout halts but does not reverse Lafora disease progression in mice. *J Biol Chem*. 2021;296:100150.
47. Varea O, Duran J, Aguilera M, Prats N, Guinovart JJ. Suppression of glycogen synthesis as a treatment for Lafora disease: Establishing the window of opportunity. *Neurobiol Dis*. 2021;147:105173.
48. Gumusgoz E, Guisso DR, Kasiri S, *et al*. Targeting Gys1 with AAV-SaCas9 decreases pathogenic polyglucosan bodies and neuroinflammation in adult polyglucosan body and lafora disease mouse models. *Neurotherapeutics*. 2021;18(2):1414–1425.
49. Ahonen S, Nitschke S, Grossman TR, *et al*. Gys1 antisense therapy rescues neuropathological bases of murine Lafora disease. *Brain*. 2021;144(10):2985–2993.
50. Peltzer N, Darding M, Montinaro A, *et al*. LUBAC is essential for embryogenesis by preventing cell death and enabling haematopoiesis. *Nature*. 2018;557(7703):112–117.
51. Tokunaga F, Sakata S, Saeki Y, *et al*. Involvement of linear polyubiquitylation of NEMO in NF-kappaB activation. *Nat Cell Biol*. 2009;11(2):123–132.
52. Kaslow HR, Lesikar DD. Isozymes of glycogen synthase. *FEBS Lett*. 1984;172(2):294–298.
53. Printen JA, Brady MJ, Saltiel AR. PTG, a protein phosphatase 1-binding protein with a role in glycogen metabolism. *Science*. 1997;275(5305):1475–1478.
54. Fong NM, Jensen TC, Shah AS, Parekh NN, Saltiel AR, Brady MJ. Identification of binding sites on protein targeting to glycogen for enzymes of glycogen metabolism. *J Biol Chem*. 2000;275(45): 35034–35039.
55. Ogawa N, Hirose Y, Ohara S, Ono T, Watanabe Y. A simple quantitative bradykinesia test in MPTP-treated mice. *Res Commun Chem Pathol Pharmacol*. 1985;50(3):435–441.
56. Berthier A, Paya M, Garcia-Cabrero AM, *et al*. Pharmacological interventions to ameliorate neuropathological symptoms in a mouse model of Lafora disease. *Mol Neurobiol*. 2016;53(2):1296–1309.
57. Nitschke F, Sullivan MA, Wang P, *et al*. Abnormal glycogen chain length pattern, not hyperphosphorylation, is critical in Lafora disease. *EMBO Mol Med*. 2017;9(7):906–917.
58. Lafora GR, Glueck B. Beitrag zur Histopathologie der myoklonischen Epilepsie. *Z Gesamte Neurol Psychiatr*. 1911; 6(1):1–14.
59. Harriman DG, Millar JH, Stevenson AC. Progressive familial myoclonic epilepsy in three families: Its clinical features and pathological basis. *Brain*. 1955;78(3):325–349.
60. Schwarz GA, Yanoff M. Lafora's disease. Distinct clinicopathologic form of Unverricht's syndrome. *Arch Neurol*. 1965; 12:172–188.
61. MacDuff DA, Reese TA, Kimmey JM, *et al*. Phenotypic complementation of genetic immunodeficiency by chronic herpesvirus infection. *eLife*. 2015;4:e04494.
62. Hedberg-Oldfors C, Oldfors A. Polyglucosan storage myopathies. *Mol Aspects Med*. 2015;46:85–100.

63. Tagliabracci VS, Girard JM, Segvich D, *et al*. Abnormal metabolism of glycogen phosphate as a cause for Lafora disease. *J Biol Chem*. 2008;283(49):33816–33825.
64. Turnbull J, Wang P, Girard JM, *et al*. Glycogen hyperphosphorylation underlies Lafora body formation. *Ann Neurol*. 2010;68(6):925–933.
65. DePaoli-Roach AA, Contreras CJ, Segvich DM, *et al*. Glycogen phosphomonoester distribution in mouse models of the progressive myoclonic epilepsy, Lafora disease. *J Biol Chem*. 2015;290(2):841–850.
66. Vilchez D, Ros S, Cifuentes D, *et al*. Mechanism suppressing glycogen synthesis in neurons and its demise in progressive myoclonus epilepsy. *Nat Neurosci*. 2007;10(11):1407–1413.
67. DePaoli-Roach AA, Tagliabracci VS, Segvich DM, Meyer CM, Irimia JM, Roach PJ. Genetic depletion of the malin E3 ubiquitin ligase in mice leads to Lafora bodies and the accumulation of insoluble laforin. *J Biol Chem*. 2010;285(33):25372–25381.
68. López-Muñoz F, Boya J, Alamo C. Neuron theory, the cornerstone of neuroscience, on the centenary of the Nobel Prize award to Santiago Ramon y Cajal. *Brain Res Bull*. 2006;70(4–6):391–405.
69. Van Heycop Ten Ham MW. Lafora disease, a form of progressive myoclonus epilepsy. In: *The epilepsies handbook of clinical neurology 15*. North-Holland Publishing Elsevier; 1974:382–422.
70. Augé E, Pelegrí C, Manich G, *et al*. Astrocytes and neurons produce distinct types of polyglucosan bodies in Lafora disease. *Glia*. 2018;66(10):2094–2107.
71. Rubio-Villena C, Viana R, Bonet J, *et al*. Astrocytes: New players in progressive myoclonus epilepsy of Lafora type. *Hum Mol Genet*. 2018;27(7):1290–1300.
72. Valles-Ortega J, Duran J, Garcia-Rocha M, *et al*. Neurodegeneration and functional impairments associated with glycogen synthase accumulation in a mouse model of Lafora disease. *EMBO Mol Med*. 2011;3(11):667–681.
73. Pederson BA, Chen H, Schroeder JM, Shou W, DePaoli-Roach AA, Roach PJ. Abnormal cardiac development in the absence of heart glycogen. *Mol Cell Biol*. 2004;24(16):7179–7187.
74. Gayarre J, Duran-Trio L, Criado Garcia O, *et al*. The phosphatase activity of laforin is dispensable to rescue Epm2a$^{-/-}$ mice from Lafora disease. *Brain*. 2014;137(3):806–818.
75. Sullivan M, Nitschke S, Steup M, Minassian B, Nitschke F. Pathogenesis of Lafora disease: Transition of soluble glycogen to insoluble polyglucosan. *Int J Mol Sci*. 2017;18(8):1743.
76. Sun RC, Young LEA, Bruntz RC, *et al*. Brain glycogen serves as a critical glucosamine cache required for protein glycosylation. *Cell Metab*. 2021;33(7):1404–1417.e9.
77. Takiuchi T, Nakagawa T, Tamiya H, *et al*. Suppression of LUBAC-mediated linear ubiquitination by a specific interaction between LUBAC and the deubiquitinases CYLD and OTULIN. *Genes Cells*. 2014;19(3):254–272.
78. Fiil BK, Gyrd-Hansen M. The Met1-linked ubiquitin machinery in inflammation and infection. *Cell Death Differ*. 2021;28(2):557–569.
79. Chen L, Wang N, Hu W, *et al*. Polyglucosan body myopathy 1 may cause cognitive impairment: A case report from China. *BMC Musculoskelet Disord*. 2021;22(1):35.
80. Hedberg-Oldfors C, Abramsson A, Osborn DPS, *et al*. Cardiomyopathy with lethal arrhythmias associated with inactivation of KLHL24. *Hum Mol Genet*. 2019;28(11):1919–1929.
81. Tang B, Frasinyuk MS, Chikwana VM, *et al*. Discovery and development of small-molecule inhibitors of glycogen synthase. *J Med Chem*. 2020;63(7):3538–3551.